



# Modeling the inflammatory response in the hypothalamus ensuing heat stroke: Iterative cycle of model calibration, identifiability analysis, experimental design and data collection



Hagen Klett<sup>a,c</sup>, Maria Rodriguez-Fernandez<sup>a,\*</sup>, Shauna Dineen<sup>b</sup>, Lisa R. Leon<sup>b</sup>, Jens Timmer<sup>c,d</sup>, Francis J. Doyle III<sup>a</sup>

<sup>a</sup> Department of Chemical Engineering, University of California – Santa Barbara, Santa Barbara, CA, USA

<sup>b</sup> Thermal and Mountain Medicine Division, US Army Research Institute of Environmental Medicine, Natick, MA, USA

<sup>c</sup> Institute of Physics, University of Freiburg, Freiburg, Germany

<sup>d</sup> BIOS Centre for Biological Signalling Studies, University of Freiburg, Freiburg, Germany

## ARTICLE INFO

### Article history:

Received 20 May 2014

Revised 30 July 2014

Accepted 31 July 2014

Available online 10 August 2014

### Keywords:

Heat stroke

Hypothalamus

Mathematical modeling

Optimal experimental design

Bayesian

## ABSTRACT

Heat Stroke (HS) is a life-threatening illness caused by prolonged exposure to heat that causes severe hyperthermia and nervous system abnormalities. The long term consequences of HS are poorly understood and deeper insight is required to find possible treatment strategies. Elevated pro- and anti-inflammatory cytokines during HS recovery suggest to play a major role in the immune response. In this study, we developed a mathematical model to understand the interactions and dynamics of cytokines in the hypothalamus, the main thermoregulatory center in the brain. Uncertainty and identifiability analysis of the calibrated model parameters revealed non-identifiable parameters due to the limited amount of data. To overcome the lack of identifiability of the parameters, an iterative cycle of optimal experimental design, data collection, re-calibration and model reduction was applied and further informative experiments were suggested. Additionally, a new method of approximating the prior distribution of the parameters for Bayesian optimal experimental design based on the profile likelihood is presented.

© 2014 Elsevier Inc. All rights reserved.

## 1. Introduction

Heat Stroke (HS) is a life-threatening illness caused by prolonged exposure to heat. It is commonly diagnosed as core temperatures ( $T_c$ ) > 40 °C, profound central nervous system abnormalities and organ or tissue damage [1]. In times of global warming, HS is not only a sports and military problem [2] but becomes a public health issue, endangering not only the young and elderly [3]. In the past two decades HS had a higher death toll in the United States than tornadoes, hurricanes, earthquakes and lightning combined [4]. Despite clinical cooling therapies, HS is often followed by the systemic inflammatory response syndrome (SIRS) and multi organ dysfunction and no preventive treatments, e.g., pharmaceuticals have been discovered [5,6]. Mechanisms mediating SIRS are not well understood, but concomitantly elevated pro- and anti-inflammatory cytokines during HS recovery [1,3–6] suggest that a complex network of cytokines functions as potential mediator. Furthermore, HS patients and animal models show unexplained

temperature behavior during recovery consisting of immediate hypothermia and fever 24 h after heat exposure. Hypothermia is thought to be a consequence of damage to the pre-optic anterior hypothalamus (POAH) [1,3], which is considered the main thermoregulatory center in the brain [7,8], however, these effects also occur in absence of any damage [6]. Elevated pro- and anti-inflammatory cytokines are able to act on the CNS to regulate  $T_c$  during inflammation which makes them most likely to be part of the  $T_c$  response. Biedenkapp et al. [6] determined increased cytokines (heat shock protein 72 (HSP), interleukin-6 (IL-6), IL-1, tumor necrosis factor (TNF)  $\alpha$ ) and cyclooxygenase (COX) 2 gene expression changes in the hypothalamus, suggesting them to be associated with SIRS and  $T_c$  regulation.

Rodriguez-Fernandez et al. [4] developed a mathematical HS model, describing the dynamics of gene expression of HSP, IL-1 $\alpha$ , IL-1 $\beta$ , IL-6, IL-10 and TNF- $\alpha$  in the liver during early stages of SIRS. To understand the cytokine dynamics which may regulate  $T_c$ , we extended the approach to the hypothalamus. In contrast to the complex model in [4] (65 ordinary differential equations (ODEs) and 130 free parameters) a more simple model was built to describe the dynamics of HSP, IL-6, TNF- $\alpha$ , IL-1, IL-10 and cox-2

\* Corresponding author.

E-mail address: [maria.rodriguez.fernan@gmail.com](mailto:maria.rodriguez.fernan@gmail.com) (Maria Rodriguez-Fernandez).

gene expression disregarding any transcription factors. A systems biology approach helps to gain insight in the important interactions and pathways during and ensuing HS as well as explains the dynamics of the observables between measurements. The mathematical model helps to identify the molecular mechanisms, which may serve as potential pharmaceutical targets in HS patients and can be utilized to perform *in silico* experiments, which saves costs, time and reduces animal testings.

In order to rely on the obtained information from the model, it is important that its predictions can be trusted. Model predictions depend on the estimated model parameters which are obtained from the fitting to the experimental data and their identifiability. After parameter estimation, some parameters may not be identifiable, due to a limited amount and quality of the experimental data. That means the confidence intervals (interval; which contains the true value with a certain probability) are infinite. Even if parameters are uniquely identifiable they can only be estimated within a finite confidence interval, in case measurement errors exist [9]. Uncertainties in the parameter estimates thus directly translate in model predictions making some biological questions not addressable [10].

Hence, it is important to resolve non-identifiabilities in a mathematical model by incorporating new data. However, the choice of new data is crucial to the information which is needed to identify parameters. Optimal experimental design (OED) can be used to find the most informative experimental conditions. In this study an iterative cycle of model calibration, identifiability analysis, OED and experiments is demonstrated to identify parameters in an inflammatory model describing the cytokine interactions in the hypothalamus. Parameter estimation is done by optimizing the likelihood and identifiability analysis as well as OED is based on the profile likelihoods of the estimates [10]. Additionally a new method of approximating the prior distribution of parameters in Bayesian OED is presented.

## 2. Methods

### 2.1. Description of the data

A detailed description of the experimental methods can be found elsewhere [6]. Briefly, male C57BL/6J mice were accustomed to standard environmental conditions ( $25 \pm 2$  °C, 12:12 h light–dark cycle, lights on at 6am). Before the experiment mice were intraperitoneally implanted with a battery-operated radiotelemetry transmitter device to record  $T_c$ .  $T_c$  was monitored in 1-min intervals with a precision of  $\pm 0.1$  °C throughout the experiment. Full recovery from surgery was awaited until experiments were begun ( $\geq 1$  week). A detailed version of the heat stress protocol can be found elsewhere [3]. In summary, mice were exposed to an ambient temperature ( $T_a$ ) of  $39.5 \pm 0.2$  °C without food and water until they reached a maximum temperature ( $T_{c,max}$ ) of 42.7 °C. Ensuing removal from the heat, mice were kept at  $T_a = 25$  °C with free access to food and water for recovery. Prior to the experiment mice were randomly assigned to one of the following groups for tissue collection: (1) baseline (immediately prior to the experiment,  $t = 0$ ), (2)  $T_{c,max}$  ( $T_c = 42.7$  °C), (3) hypothermia depth (HD; lowest  $T_c$  value with cooling rate  $\leq 0.01$  °C/min) and (4) 24 h after heat exposure. RNA was isolated from micropunches of the hypothalamus and cDNA was synthesized which was used in real-time PCR (polymerase chain reaction) experiments. For each gene a threshold cycle (Ct) was defined as the PCR cycle where the emitted fluorescence signal was greater than any background noise. Data of heated and non-heated controls were normalized by calculating the difference in Ct values between the target gene of interest and the 18s internal housekeeping gene

$$\Delta Ct = Ct_{target} - Ct_{18sRNA}. \quad (1)$$

Gene expression changes in heated mice were calculated as fold changes relative to the average of non-heated controls using the  $2^{-\Delta\Delta Ct}$  method [11] at the specific time points ( $T_{c,max}$ , HD, 24 h) with

$$\Delta\Delta Ct = \Delta Ct_{heated} - \Delta Ct_{av.control}. \quad (2)$$

Furthermore the mean of the fold changes and its standard error was calculated at every time point  $t_j$  ( $T_{c,max}$ , HD, 24 h) for all observables  $i$  (HSP, IL-6, IL-1 $\beta$ , TNF- $\alpha$ , cox-2) according to

$$\bar{y}_i(t_j) = \frac{1}{Z} \sum_{z=1}^Z \tilde{y}_{iz}(t_j) \text{ and } \sigma_i(t_j) = \frac{\sigma_{\tilde{y}_{iz}}(t_j)}{\sqrt{Z}} \quad (3)$$

with

$$\sigma_{\tilde{y}_{iz}}(t_j) = \sqrt{\frac{1}{Z-1} \sum_{z=1}^Z (\tilde{y}_{iz}(t_j) - \bar{y}_i(t_j))^2}. \quad (4)$$

and  $Z$  being the number of data points obtained at  $t_j$ . A detailed description of the data is provided in [6] and summarized in Table 1.

In order to use the mean fold changes calculated in Eq. (3) an average of the temperature profiles of the heated mice has to be used. However, sampling points at  $T_{c,max}$  and HD depend on the temperature and therefore vary in the sampling times according to the individual heating and cooling rate of the mice. Rodriguez-Fernandez et al. [4] has shown that averaging along the time axis would lead to misleading results in terms of the temperature values. Thus individual temperature profiles were averaged along the temperature axis (Fig. 1). For modeling purposes sampling time points at  $T_{c,max}$  and HD were determined from the averaged temperature profile to  $t_{T_{c,max}} = 261$  min and  $t_{HD} = 445$  min.

### 2.2. Framework, modeling and assumptions

The underlying framework of the mathematical model describing the cytokine dynamics during heat stroke is presented in Fig. 2. The dynamics are modeled by ODEs

$$\frac{d}{dt} \mathbf{x}(t, \boldsymbol{\theta}) = \mathbf{f}(\mathbf{x}, \boldsymbol{\theta}, u(t)) \quad (5)$$

where  $\mathbf{x}$  is a vector of the species,  $\boldsymbol{\theta}$  the free model parameters and  $u(t)$  an input to the system.  $\mathbf{f}$  describes all reaction rates and inputs to the respective species. It will be specified in the following.

It has been assumed that the elevated  $T_c$  is the only trigger of the concomitantly elevated pro- and anti-inflammatory cytokines by increasing the concentration of denatured proteins, endotoxins (lipopolysaccharides, LPS) and reactive oxygen species (ROS) [4]. Seeing that NF- $\kappa$ B is not strongly elevated during heat stroke in the liver [4] and the fact of increased mortality in toll-like receptor 4 (TLR4; receptor to detect LPS and initiate an immune response) KO mice [12] suggests that LPS may not play a significant role. Furthermore we neglected the impact of ROS and tested the hypothesis that immune responses ensuing heat stroke are mainly mediated by denatured proteins. Denaturation of proteins can

**Table 1**

Data shows fold changes in the hypothalamus of heated relative to controls in C57BL/6J mice.

Gene	$T_{c,max}$	HD	24 h
HSP	44 $\pm$ 12 <sup>a</sup>	216 $\pm$ 18 <sup>a</sup>	1.0 $\pm$ 0.5
IL-6	1.1 $\pm$ 0.3	3.6 $\pm$ 1.1 <sup>a</sup>	0.72 $\pm$ 0.50
TNF	1.9 $\pm$ 1.3	7.8 $\pm$ 1.9 <sup>a</sup>	2.7 $\pm$ 0.6
IL-1	3.7 $\pm$ 0.8 <sup>a</sup>	27 $\pm$ 5.3 <sup>a</sup>	2.5 $\pm$ 0.9
cox2	1.5 $\pm$ 0.5	3.6 $\pm$ 0.5 <sup>a</sup>	2.0 $\pm$ 0.7

<sup>a</sup> Represents significant difference from controls (student's T-test:  $p < 0.05$ ). Data obtained from [6].

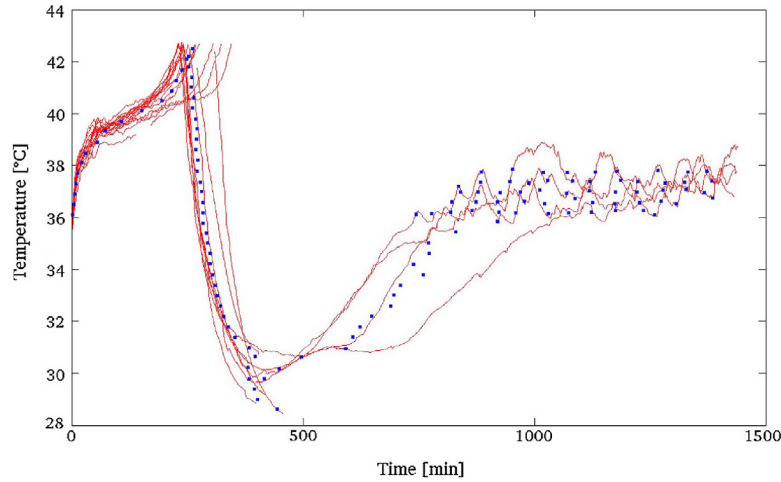


**Fig. 1.** The individual temperature profiles for the wild-type (WT) mice are shown in red and the average over temperature is displayed as a blue dotted line. (For interpretation of the references to color in this figure legend, the reader is referred to the web version of this article.)

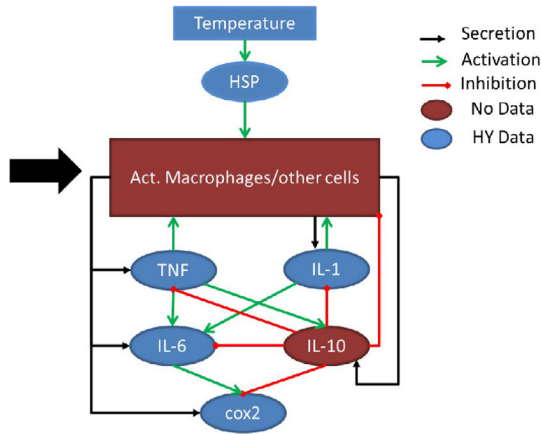


**Fig. 2.** Model of the inflammatory network of cytokines in the hypothalamus. The thick black arrow represents the activation rate coming from a constant pool of inactivated macrophages, etc. Thin black arrows represent the synthesis of mRNA coming from activated macrophages, green arrows indicate activation while red lines specify inhibition. Hypothalamus mRNA fold changes at  $T_{c,max}$ , HD and 24 h and a temperature profile were measured for blue boxes whereas no data was available for brown boxes. (For interpretation of the references to color in this figure legend, the reader is referred to the web version of this article.)

occur at temperatures as low as 37–38 °C which stimulates the expression of HSPs through activation of HSF-1 (transcription factor of HSPs) [4,13,14]. Peper et al. [14] has shown that the denaturation process of proteins is exponential in  $T_c$ . For sake of parsimony and simplicity the activation process of HSPs was disregarded and an exponential ansatz was assumed for the mRNA synthesis

$$\text{Rate of synthesis} = k_{HSP} \exp[\alpha(T_c(t) - 37^\circ\text{C})] \quad \text{for } T_c \geq 37^\circ\text{C} \quad (6)$$

where  $T_c(t)$  is the input of the system ( $u(t)$ ). It can be seen that the HSP gene expression is delayed compared to the temperature response which is most likely due to the chain of reactions starting at the denaturation of proteins until the transcription of HSP mRNA. The delay was determined to be  $\delta = 100$  min from [4] and mathematically realized as

$$T_c(t) = \begin{cases} 37^\circ\text{C}, & t < \delta, \\ T_c^*(t - \delta), & t \geq \delta. \end{cases} \quad (7)$$

To simplify the handling of the input temperature, cubic splines were fitted to the experimental data prior to computational

analysis. Cubic splines are continuous and easily to be derived, which help the usage in solving ODEs and derivative based optimization (Section 3).

Increased HSP gene expression is able to modulate the activation of macrophages and monocytes [15,16] which further can secret pro- and anti-inflammatory cytokines. Activated macrophages and monocytes are part of a black box in the model which initiates the immune response under heat stroke. It is assumed that the black box is activated from a constant pool  $M_R = 1$  of inactivated macrophages, monocytes, etc. Synthesis of mRNA was modeled with mass action kinetics proportional to the concentration of the activated black box [17]

$$\text{Rate of synthesis} = \theta_{x_i} \cdot M. \quad (8)$$

Furthermore cytokines interact with each other what can enhance or suppress the synthesis rate

$$\text{Rate of synthesis} = \theta_{x_i} \cdot M \cdot (1 + \text{Activation}) \cdot \text{Inhibition}. \quad (9)$$

For the sake of simplicity activation and inhibition are modeled with Michaelis Menten (MM) kinetics [4,17]. Activating MM kinetics are given as

$$\frac{x_j/\theta_{x_i x_j}}{1 + x_j/\theta_{x_i x_j}} \quad (10)$$

where  $x_j$  activates  $x_i$  and  $\theta_{x_i x_j}$  is the respective MM constant. Inhibiting MM kinetics are given as

$$\frac{1}{1 + x_k/\theta_{x_i x_k}} \quad (11)$$

Here,  $x_k$  inhibits  $x_i$  and  $\theta_{x_i x_k}$  is the inhibiting MM constant. Last but not least degradation is assumed to be linear, i.e.,

**Table 2**  
Table of interactions with corresponding references and assumptions.

Gene	Synthesis and production	Activation by MM kinetics	Inhibition by MM kinetics
HSP	$T_c$ dependent [14]	–	–
M	Const. $M_R = 1$	HSP [15], TNF [18,19], IL-1 [18]	IL-10 [20]
IL-6	$\propto M$ [21]	TNF [22,23], IL-1 [22]	IL-10 [20]
TNF	$\propto M$ [24]	–	IL-10 [20]
IL-10	$\propto M$ [25]	TNF [26,24]	–
IL-1	$\propto M$ [27]	–	IL-10 [20]
cox-2	$\propto M$ [28]	IL-6 [29–31]	IL-10 [20]

$$\text{Rate of degradation} = d_{x_i} \cdot x_i. \quad (12)$$

The considered interactions in the model are shown in Fig. 2 and are summarized in Table 2.

Thus the full set of ODEs reads as follows:

$$\begin{aligned} \frac{dHSP}{dt} &= \theta_{HSP} e^{\alpha(T(t)-37)} - d_{HSP} HSP \\ \frac{dM}{dt} &= M_R \cdot \left( \frac{HSP/\theta_{MHSP}}{1 + HSP/\theta_{MHSP}} + \frac{IL1/\theta_{MIL1}}{1 + IL1/\theta_{MIL1}} + \frac{TNF/\theta_{MTNF}}{1 + TNF/\theta_{MTNF}} \right) \\ &\quad - d_M M \\ \frac{dIL6}{dt} &= \theta_{IL6} \cdot M \cdot \left( 1 + \frac{TNF/\theta_{IL6TNF}}{1 + TNF/\theta_{IL6TNF}} + \frac{IL1/\theta_{IL6IL1}}{1 + IL1/\theta_{IL6IL1}} \right) \\ &\quad - d_{IL6} IL6 \\ \frac{dTNF}{dt} &= \theta_{TNF} \cdot M \cdot \frac{1}{1 + IL10/\theta_{TNFIL10}} - d_{TNF} TNF \\ \frac{dIL10}{dt} &= \theta_{IL10} \cdot M \cdot \left( 1 + \frac{TNF/\theta_{IL10TNF}}{1 + TNF/\theta_{IL10TNF}} \right) - d_{IL10} IL10 \\ \frac{dIL1}{dt} &= \theta_{IL1} \cdot M \cdot \frac{1}{1 + IL10/\theta_{IL1IL10}} - d_{IL1} IL1 \\ \frac{dcox2}{dt} &= \theta_{cox2} \cdot M \cdot \left( 1 + \frac{IL6/\theta_{cox2IL6}}{1 + IL6/\theta_{cox2IL6}} \right) * \frac{1}{1 + IL10/\theta_{cox2IL10}} - d_{cox2} cox2. \quad (13) \end{aligned}$$

Here, the free parameters combine to a parameter vector  $\theta$  and the degradation constants are denoted by  $d$  with appropriate subscripts.

Without heat the system of ODEs is assumed to be at steady state

$$\frac{d}{dt} \mathbf{x}(t, \theta) = 0. \quad (14)$$

Fold changes of gene expression of heated mice are calculated relative to controls, i.e., initial conditions that are equivalent to steady state conditions are  $\mathbf{x}_0 = \mathbf{1}$  for all compounds of the model. Degradation constants can therefore be calculated as

$$\left\{ d_{x_i} : \frac{\dot{x}_i(t=0, \theta)}{dt} = 0 \right\} \quad (15)$$

and the number of estimated parameters is reduced from 26 to 19.

### 3. Computational methods

#### 3.1. Model calibration

The system of ODEs has been solved numerically by CVODES [32] which can be accessed by a MATLAB interface and simultaneously provides derivatives of the estimates which are needed in the optimization.

The model parameters  $\theta$  have been estimated by optimizing the likelihood estimator. Assuming normally distributed measurement noise the likelihood function

$$L(\tilde{\mathbf{y}}|\theta) = \prod_{k=1}^{N_k} \prod_{i=1}^{N_i} \prod_{j=1}^{N_j} \frac{1}{\sqrt{2\pi} \sigma_{ik}(t_j)} \exp \left[ -\frac{(\tilde{y}_{ik}(t_j) - y_{ik}(t_j, \theta))^2}{2\sigma_{ik}^2(t_j)} \right] \quad (16)$$

is a well-known distance measure. Here,  $N_k$  is the number of experiments,  $N_i$  the number measured observables and  $N_j$  the number of sampling points,  $\tilde{y}_{ik}(t_j)$  is the measurement  $i$  in experiment  $k$  at time  $t_j$ ,  $y_{ik}(t_j, \theta)$  the predicted model value  $i$  in experiment  $k$  at time  $t_j$  and  $\sigma_{ik}(t_j)$  the respective variance of the measurement. Maximizing the likelihood function is equivalent to minimizing the weighted sum of squared residuals

$$\chi^2(\tilde{\mathbf{y}}|\theta) = \sum_{ijk} \frac{(\tilde{y}_{ik}(t_j) - y_{ik}(t_j, \theta))^2}{\sigma_{ik}^2(t_j)}. \quad (17)$$

The optimization

$$\hat{\theta} = \arg \min_{\theta} \chi^2(\tilde{\mathbf{y}}|\theta) \quad (18)$$

has been performed with the implemented MATLAB function LSQNONLIN. It is a local deterministic solver based on the gradient

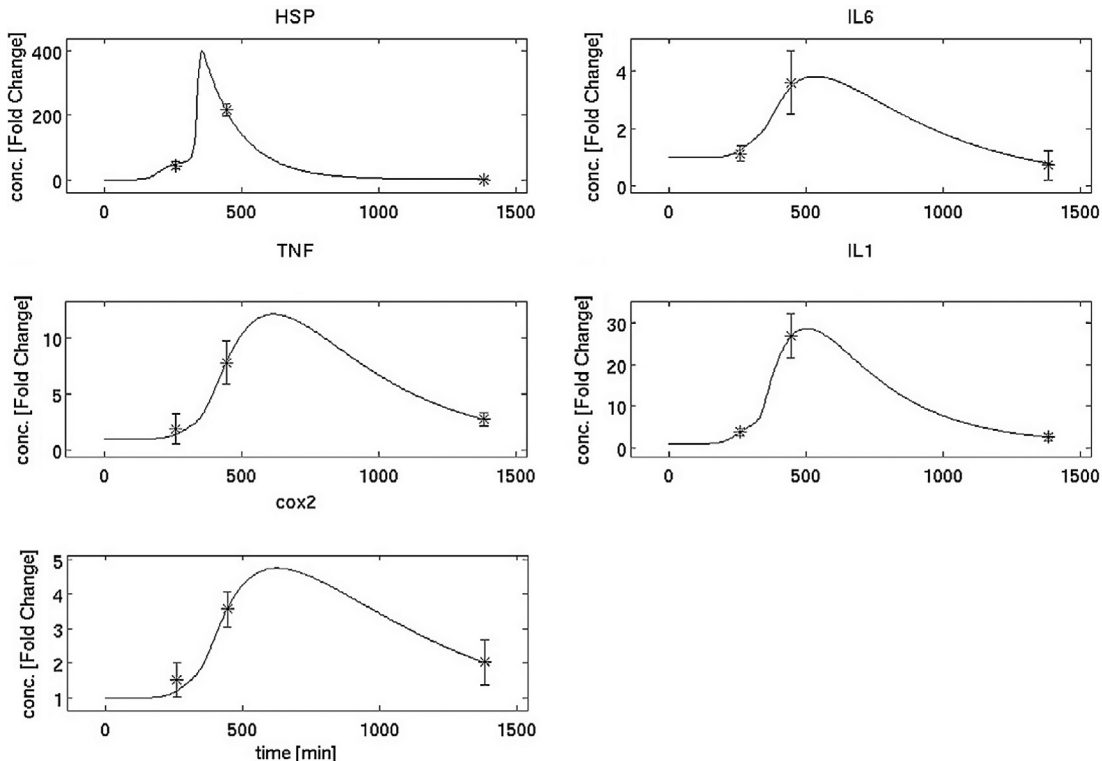
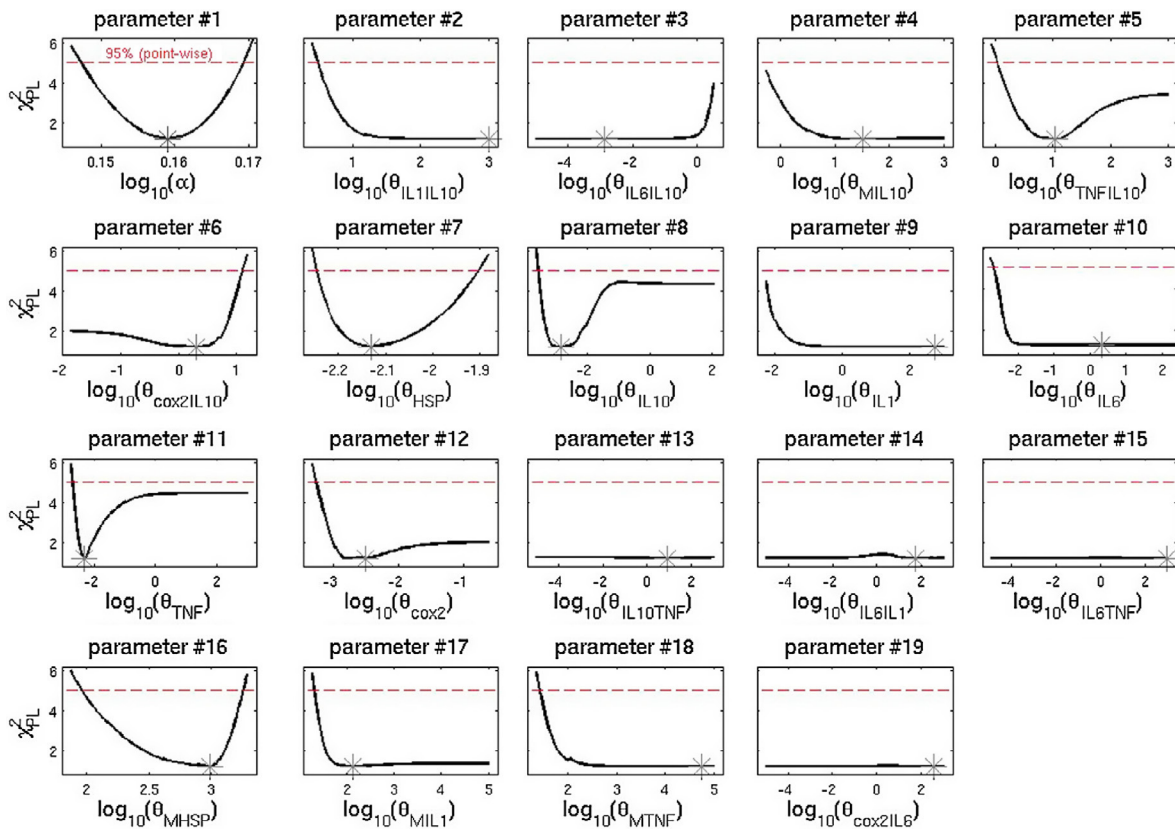


Fig. 3. The heat stroke model (solid lines) was calibrated to gene expression data from HSP, IL-6, TNF, IL-1 and cox-2 at  $T_{c,max}$ , HD and 24 h. Data is indicated with an asterisk and one standard deviation is plotted by error bars. Initial conditions were given by controls  $\mathbf{x}_0 = \mathbf{1}$ .



**Fig. 4.** Profile likelihoods  $\chi^2_{PL}(\theta_i)$  (black solid lines) were calculated for 19 model parameters with respect to the WT data. A 95% point-wise threshold (red dashed line) holds for each parameter individually ( $df = 1$ ). The optimal parameter value is indicated with an asterisk. (For interpretation of the references to colour in this figure legend, the reader is referred to the web version of this article.)

of the cost function. To avoid local minima a multistart method has been used where initial parameters were generated with Latin hypercube sampling [33].

### 3.2. Identifiability analysis

Identifiability of the parameters was analyzed by calculating the profile likelihood of each parameter [10,34]

$$PL(\theta_m) = \min_{\theta_{n \neq m}} \chi^2(\tilde{\mathbf{y}}|\theta). \quad (19)$$

by re-optimizing  $\chi^2(\tilde{\mathbf{y}}|\theta)$  with respect to  $\theta_{n \neq m}$  for different values of  $\theta_m$ . It breaks down the high dimensional parameter space into one dimension and makes identifiability easy to visualize. A perfectly flat

profile indicates a structural non-identifiable parameter, i.e., it depends on the model structure only and cannot be resolved by increasing the amount or quality of the data. A desired confidence level has been used to distinguish between practical non-identifiable and identifiable parameters. For identifiable parameters the confidence interval is finite whereas for practical non-identifiable parameters it is infinite on either or both the upper and lower bound. The confidence interval can be obtained from the profile likelihood

$$CI(\theta_m) = \{\theta_m | PL(\theta_m) \leq \chi^2(\tilde{\mathbf{y}}|\theta)^* + \Delta_\alpha\} \quad (20)$$

where  $\Delta_\alpha$  is the  $\alpha$ -quantile of the  $\chi^2$  inverse cumulative distribution function with one degree of freedom and  $\chi^2(\tilde{\mathbf{y}}|\theta)^*$  the optimized cost function with respect to all parameters. In this work a

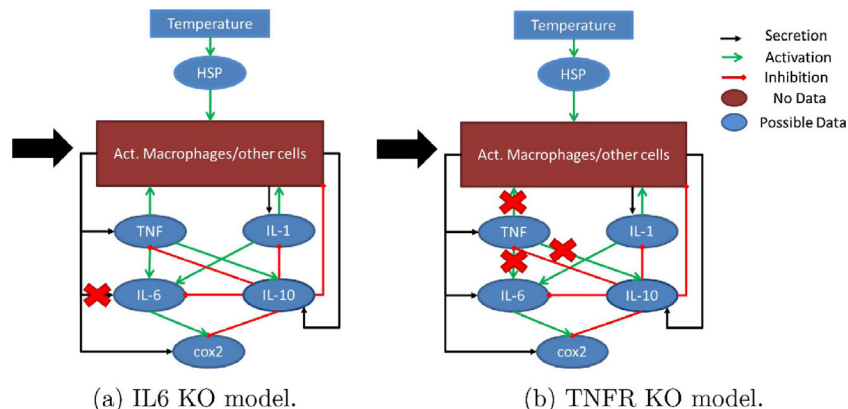
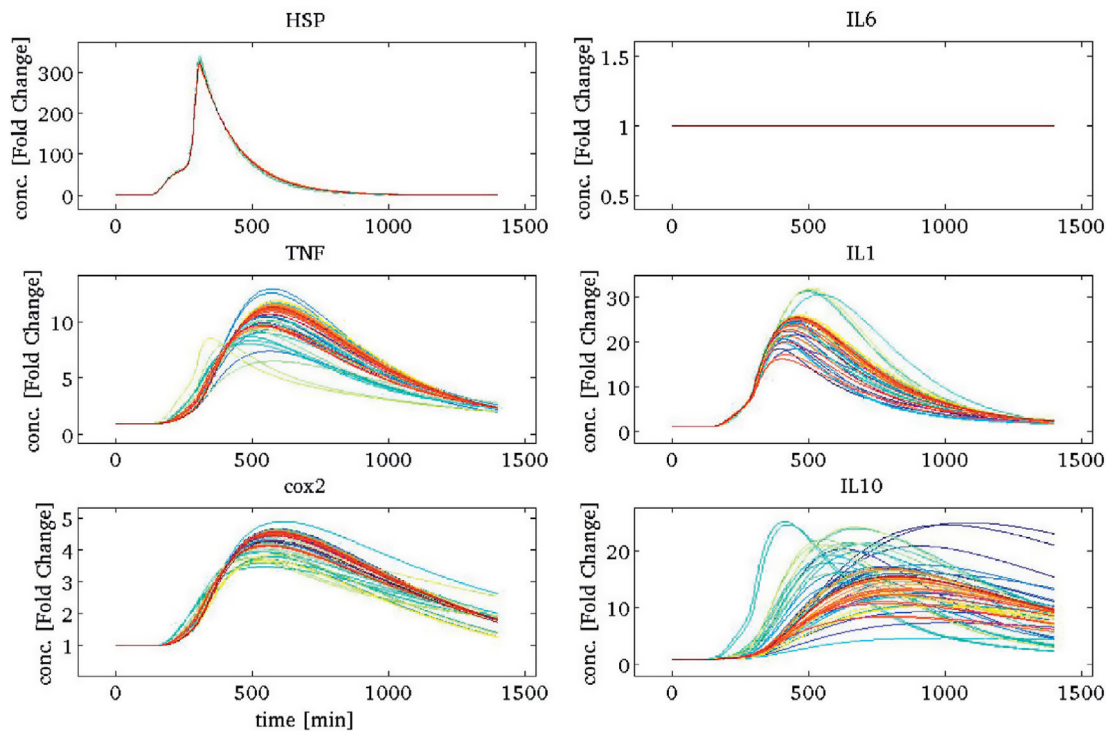
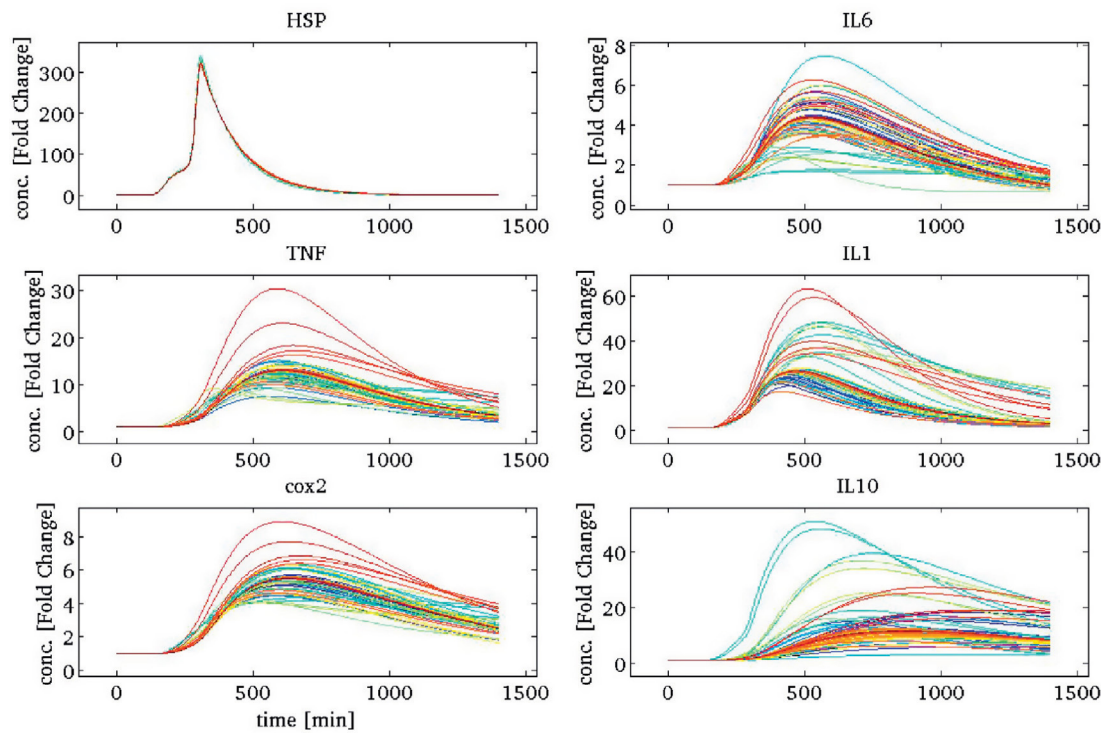


**Fig. 5.** Modifications of the inflammatory pathways in the knock out experiments are indicated with a red cross. (For interpretation of the references to color in this figure legend, the reader is referred to the web version of this article.)



(a) IL6 KO



(b) TNFR KO

**Fig. 6.** To perform OED with the trajectory method, parameter vectors were chosen along the profile likelihoods of non-identifiable parameters (Fig. 4). Then model predictions of knock out designs were simulated for the possible observables HSP, IL-6, TNF, IL-1, cox-2 and IL-10. A large spread indicates an informative measurement and a small spread a weak informative experiment.

threshold corresponding to a 95% ( $\alpha = 0.95$ ) confidence level has been chosen.

Model calibration and identifiability analysis were performed with the open source software D2D [33] which can be obtained from <https://bitbucket.org/d2d-development/d2d-software/overview>.

### 3.3. Optimal experimental design

OED can be used to choose among possible experiments  $\omega$  such that the free model parameters  $\theta$  can be optimally estimated from the measurement data  $\tilde{y}(\omega)$  which becomes a function of  $\omega$ . The

OED problem aims to find the most informative experiment  $\hat{\omega}$  within a design space  $\Omega$ .

A common approach is to maximize a scalar measure  $\phi(\cdot)$  of the Fisher Information Matrix (FIM) [35,36]

$$\hat{\omega} = \operatorname{argmax}_{\omega \in \Omega} \phi(\operatorname{FIM}(\omega, \theta)). \quad (21)$$

where the FIM quantifies the information content of the experimental data and is defined as the expectation of the second derivative of the log-likelihood with respect to the change of parameters [35]. If the parameter estimates are normally distributed the FIM

$$\operatorname{FIM}_{nm}(\omega, \theta) = \sum_{ijk} \frac{1}{\sigma_{ik}^2(t_j)} \frac{\partial^2 y_{ik}(t_j, \theta)}{\partial \theta_n \partial \theta_m} \quad (22)$$

contains second order derivatives of the observables with respect to the free parameters. For the scalar measurement  $\phi(\cdot)$  the commonly “alphabetical” OED criteria were used. A-optimal maximizes the sum of eigenvalues of the FIM which corresponds to minimizing the average variance of the estimated parameters. D-optimal minimizes the generalized variance of the estimated parameters by maximizing the determinant of the FIM and E-optimal minimizes the estimate with the largest uncertainty by maximizing the smallest eigenvalue. In nonlinear dynamic systems, the FIM depends on the estimated model parameters  $\theta$  and therefore makes it only meaningful if all parameters are identifiable [35]. In the presence of non-identifiabilities robust OED methods are needed.

### 3.3.1. Bayesian OED

Bayesian OED considers the prior probability distribution  $P(\theta)$  of the parameters. Based on Lindleys decision theory framework [37], He et al. [36] presented a general Bayesian design criterion

$$\hat{\omega} = \operatorname{argmax}_{\omega \in \Omega} \mathbb{E}_{\theta \in \Theta} \{ \phi(\operatorname{FIM}(\omega, \theta)) \} \quad (23)$$

$$= \operatorname{argmax}_{\omega \in \Omega} \int_{\Theta} \phi(\operatorname{FIM}(\omega, \theta)) P(\theta) d\theta. \quad (24)$$

Applying the design criteria  $\phi(\cdot)$  as discussed in the previous section the approach is straightforward. However, for most biological networks the prior parameter distribution  $P(\theta)$  is unknown and has to be assumed. The prior has been realized in literature as e.g. a multivariate uniform distribution in the parameter space  $\Theta$ , a multivariate Gaussian distribution around the estimated parameters  $\theta \sim N(\hat{\theta}, \sigma)$  [36] and a multivariate uniform logarithmic distribution in the parameter space  $\Theta$  [38]. If preceding experiments are available gathered information about estimated parameters should be used in the construction of  $P(\theta)$ . For this reason an empirical Bayesian approach is presented. Rodriguez-Fernandez et al. [38] suggested to compute the maximum likelihood function for a discrete number of parameter sets

$$L(\tilde{y}|\theta_q) : \theta_q \in \Theta \quad \text{with} \quad q = 1, 2, \dots, N \quad (25)$$

and weigh the parameter sets  $\theta_q$  accordingly

$$P(\theta_q) = \frac{L(\tilde{y}|\theta_q)}{\sum_{q=1}^N L(\tilde{y}|\theta_q)}. \quad (26)$$

Therefore one obtains a normalized discretized probability distribution

$$\sum_{q=1}^N P(\theta_q) = 1 \quad (27)$$

which converges to a continuous parameter distribution for  $N \rightarrow \infty$ . For large parameter spaces  $N$  has to be really large to obtain a meaningful prior distribution. To reduce the computational effort we decided to consider only a subspace of parameters  $\Theta_{sub} \subset \Theta$  which is in good agreement with the experimental data  $\tilde{y}$ . Therefore

parameter sets having a negligible impact on the prior distribution are ignored from the beginning. Finding such a subset can be done with the help of the profile likelihoods as defined in [39].

$$\hat{\theta}(\theta_m) = \operatorname{argmax}_{\theta_{n \neq m}} \chi^2(\tilde{y}|\theta) \quad (28)$$

is one point on the profile likelihood  $PL(\theta_m)$  which is represented by a parameter vector containing the re-optimized parameters  $\theta_{n \neq m}$  to the parameter value  $\theta_m$ . The subspace can be written as

$$\Theta_{sub} = \bigcup_m \{ \hat{\theta}(\theta_m) | \theta_m \in CI_{\alpha}(\theta_i) \} \quad (29)$$

and is visualized as all the points on the profile likelihoods beneath the threshold  $\Delta_{\alpha}$ .

$N_{sub}$  equally spaced parameter sets are chosen and weighted as in Eq. (26) along the profile likelihoods  $PL(\theta_m)$ . The new probability distribution based on the subset is given as

$$\sum_{q=1}^{N_{sub}} \sum_{m=1}^M P(\hat{\theta}_q(\theta_m)) = 1 \quad (30)$$

with  $M$  denoting the dimension of the parameter space and

$$P(\hat{\theta}_q(\theta_m)) = \frac{L(\tilde{y}|\hat{\theta}_q(\theta_m))}{\sum_{q,m} L(\tilde{y}|\hat{\theta}_q(\theta_m))}. \quad (31)$$

Inserting Eq. (31) into Eq. (24) leads back to the Bayesian OED maximization problem

$$\hat{\omega} = \operatorname{argmax}_{\omega \in \Omega} \sum_{q=1}^{N_{sub}} \sum_{m=1}^M \phi(\operatorname{FIM}(\omega, \theta)) \frac{L(\tilde{y}|\hat{\theta}_q(\theta_m))}{\sum_{q,m} L(\tilde{y}|\hat{\theta}_q(\theta_m))}. \quad (32)$$

Even though the FIM is calculated from the local sensitivities a wide range of parameters depending on its uncertainties calculated from the profile likelihoods has been considered which makes the Bayesian design robust to non-identifiabilities. Note, that the maximum range is limited to the choice of the parameter bounds.

### 3.3.2. Trajectory OED

In contrast to calculating the FIMs one can simulate the time series from the parameter vectors along the profile likelihoods for different designs  $y_{\omega}(\hat{\theta}_q(\theta_m), t)$ . The method has been described in detail in [39,10]. Briefly, a wide spread of trajectories corresponds to a very informative experiment to identify the respective parameter whereas small variability relates to a weak informative experiment. The variability of the trajectories was determined by

**Table 3**

Relative distances of predicted trajectories to the optimal trajectory along profile likelihoods of non-identifiable parameters. Distances  $S(y_i)$  were calculated according to Eq. (33) for observables in the knock out experiments. Suggested observables are indicated in red.

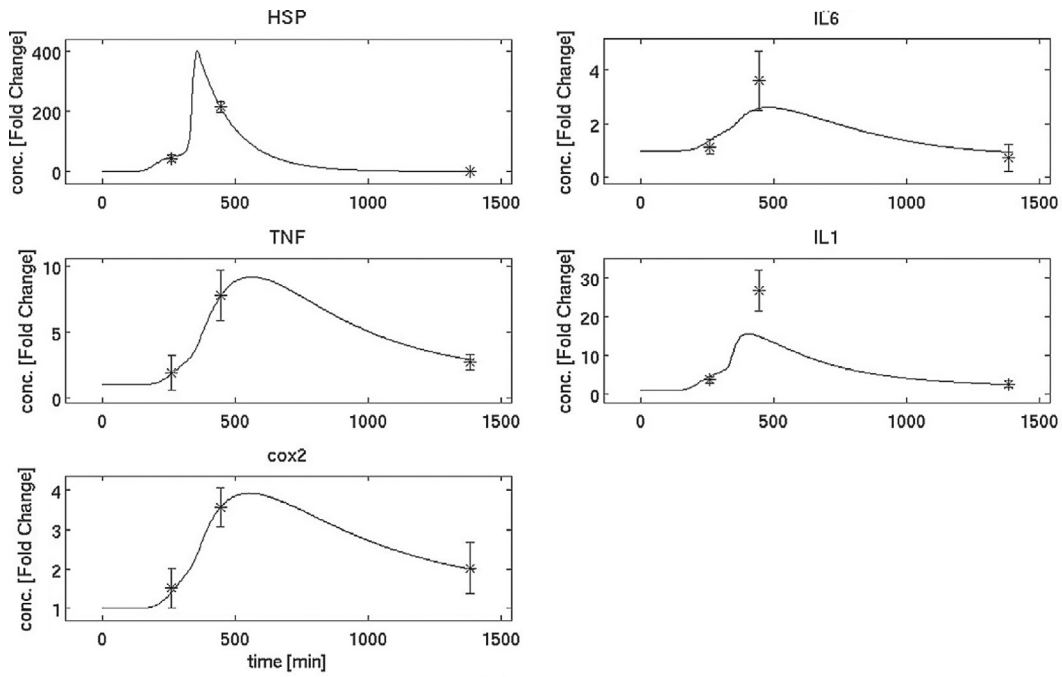
$y_i$	HSP	IL-6	TNF	IL-10	IL-1	cox-2
$S(y_i)$ IL6 KO	0.246	0	6.903	20.481	3.667	3.863
$S(y_i)$ TNFR KO	0.495	8.692	16.779	43.136	10.676	9.482
Best KO	TNFR	TNFR	TNFR	TNFR	TNFR	TNFR

**Table 4**

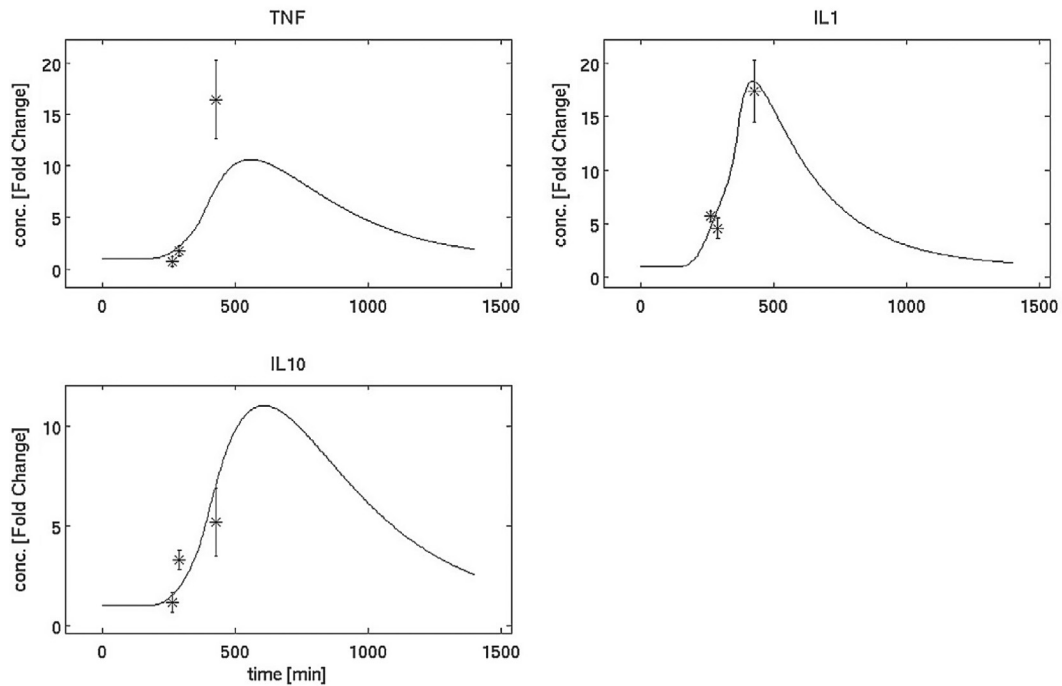
TNFR KO data in fold changes in the hypothalamus of heated mice relative to controls.

Gene	$T_{c,max}$	RTB	HD
IL-10	1.2 ± 0.5 <sup>a</sup>	3.3 ± 0.5 <sup>a</sup>	5.2 ± 1.7 <sup>a</sup>
TNF	0.7 ± 0.5	1.8 ± 0.5	16.5 ± 3.8 <sup>a</sup>
IL-1	5.7 ± 0.5 <sup>a</sup>	4.6 ± 0.9 <sup>a</sup>	17.4 ± 2.9 <sup>a</sup>

<sup>a</sup> Represents significant difference from controls (student's *T*-test:  $p < 0.05$ ).



(a) WT data



(b) TNFR KO data

**Fig. 7.** Model simulations (solid lines) versus experimental data. The heat stroke model was calibrated to WT average data at  $T_{c,max}$ , HD and 24 h and TNFR KO data at  $T_{c,max}$ , RTB and HD with initial conditions  $\mathbf{x}_0 = \mathbf{1}$ .

calculating the relative distance with respect to the optimal trajectory

$$S(y_i) = \sum_{m=1}^M \sum_{j=1}^{N_j} \sum_{q=1}^{N_{sub}} \frac{\text{abs} \left[ y_i(t_j, \hat{\theta}_q(\theta_m)) - y_i(t_j, \hat{\theta})^* \right]}{y_i(t_j, \hat{\theta}_q(\theta_m)) + y_i(t_j, \hat{\theta})^*}. \quad (33)$$

Here  $y_i(t_j, \hat{\theta})^*$  is the trajectory based on the parameter set with all parameters optimized. A large value in the cost function indicates

an informative experiment and a small value a weakly informative experiment.

## 4. Results wild type data

### 4.1. Model calibration and identifiability analysis

The mathematical model described in the previous section consists of 7 ODEs and 19 free model parameters. Experimental data of

wild-type (WT) mice were used to calibrate the model parameters. An accurate data-to-model agreement could be achieved with the model predictions lying within one confidence interval of all data points (Fig. 3). To investigate the uncertainty in the parameter estimates, the profile likelihood of each parameter was calculated where only 3 out of 19 parameters could be identified with a finite confidence interval (Fig. 4). The identifiable parameters  $\alpha$ ,  $\theta_{HSP}$  and  $\theta_{MHSP}$  are all affiliated with the dynamics of HSP gene expression, which suggests that the HSP dynamics are well-defined by the data. The other parameters are non-identifiable, i.e., the profile likelihood does not exceed the 95% threshold at either or both the lower and upper bound. The high uncertainties in the non-identifiable parameters translate into the model predictions, making them unreliable. Therefore a cycle of identifiability analysis, experimental design and experiments was chosen to improve the uncertainties in the estimates and thus the model predictions.

#### 4.2. Optimal experimental design options

Performing new experiments is very time consuming and expensive. Therefore it is important to plan a new experiment efficiently. To limit the costs as much as possible, we accessed a tissue bank of heat stroke experiments conducted with gene knock out mice. The development of knock out experiments provide a valuable tool to study cytokine interactions. Knock out mice lack functional genes for cytokines or cytokine receptors in all the tissues of the body. Giving the fact that mice survive with the lack of one gene until adulthood, one must assume that other mechanisms compensate for the absence, which make results difficult to interpret and to implement in the model.

The tissue bank contained IL6 gene knock out (IL6 KO) and TNF Receptor knock out (TNFR KO) tissues of the hypothalamus which

were frozen at  $-80\text{ }^\circ\text{C}$ . All observables except the activated black box (HSP, IL-6, TNF, IL-10, IL-1 and cox-2) of our model were possible measurements, however, due to experimental limitations only three observables could be measured. Tissue samples of heated and control mice were maintained at  $T_{c,max} = 42.4\text{ }^\circ\text{C}$ , return to baseline (RTB; first time point when  $T_c$  falls below  $36\text{ }^\circ\text{C}$  during recovery) and HD.

IL6 KO mice lack IL-6 congenitally in all tissues and are not able to produce IL-6 gene expression in any way. Mathematically, the design has been realized by setting the secretion rate and the degradation rate of IL-6 to zero ( $k_{IL6} = d_{IL6} = 0$ ; Fig. 5a), thus no other compensating mechanisms were considered. TNFR KO mice lack all the TNF Receptors (p55 and p75), meaning they are not able to induce any biological effects outgoing from TNF. However, that does not mean that TNF cannot be expressed. Mathematically all the interactions terms outgoing from TNF were consequently removed in the system of ODEs (see Fig. 5b).

##### 4.2.1. Optimal experimental design results

OED was performed to find the most informative experiment among IL6 KO and TNFR KO mice to identify the non-identifiable parameters of the mathematical model. Our novel empirical Bayesian OED favored TNFR KO for all criteria. To identify the most important observables individually the trajectory method was regarded. Five trajectories per profile likelihood along non-identifiable parameters were simulated according to the respective design. Results are illustrated in Fig. 6 and summarized in Table 3.

The relative spreads of trajectories were calculated at the time points  $T_{c,max}$  ( $t = 261\text{ min}$ ), RTB ( $t = 290\text{ min}$ ) and HD ( $t = 445\text{ min}$ ), revealing TNF, IL-10 and IL-1 as most informative observables to measure. Analyzing Fig. 6, the largest spread of trajectories occurs during recovery from HD, i.e.,  $t \approx 500\text{--}700\text{ min}$ .

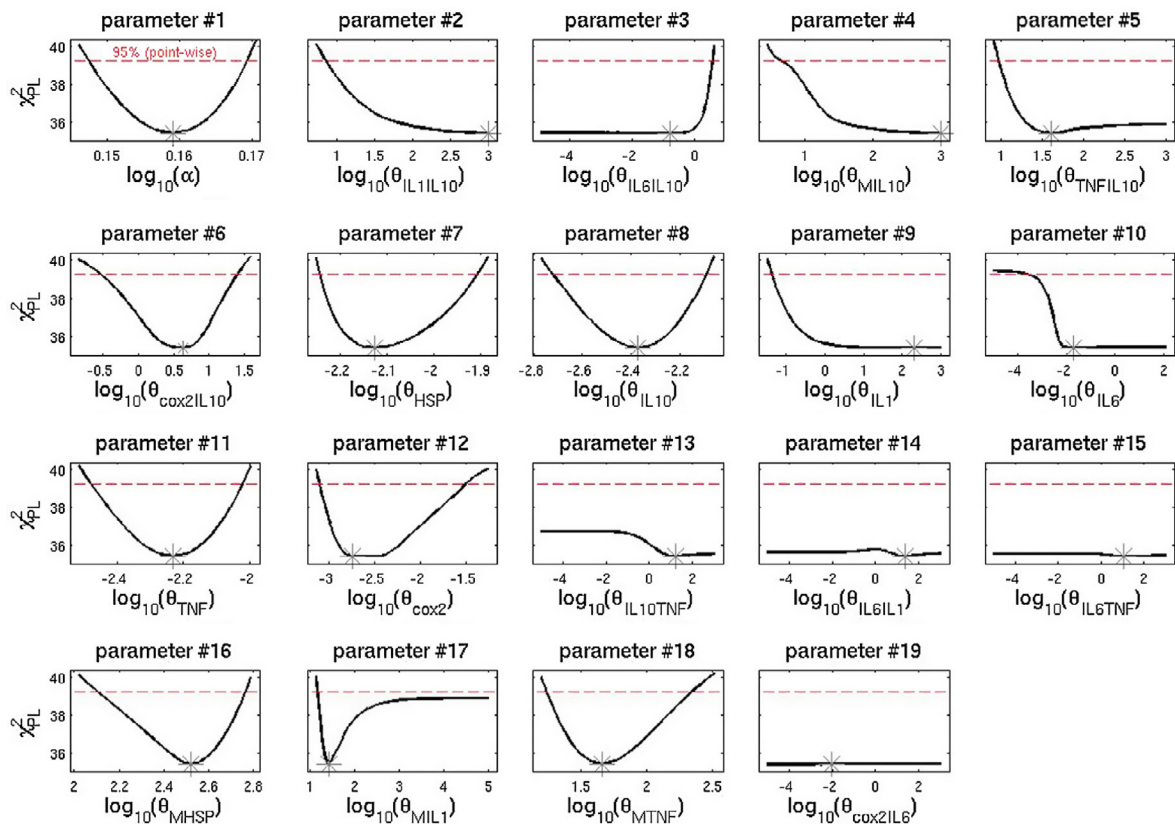


**Fig. 8.** Profile likelihoods  $\chi^2_{pL}$  of the model parameter (solid lines) including the **WT and the TNFR KO data**. A 95% point-wise threshold (red dashed line) holds for each parameter individually ( $df = 1$ ). The optimal parameter value is indicated with an asterisk. (For interpretation of the references to color in this figure legend, the reader is referred to the web version of this article.)

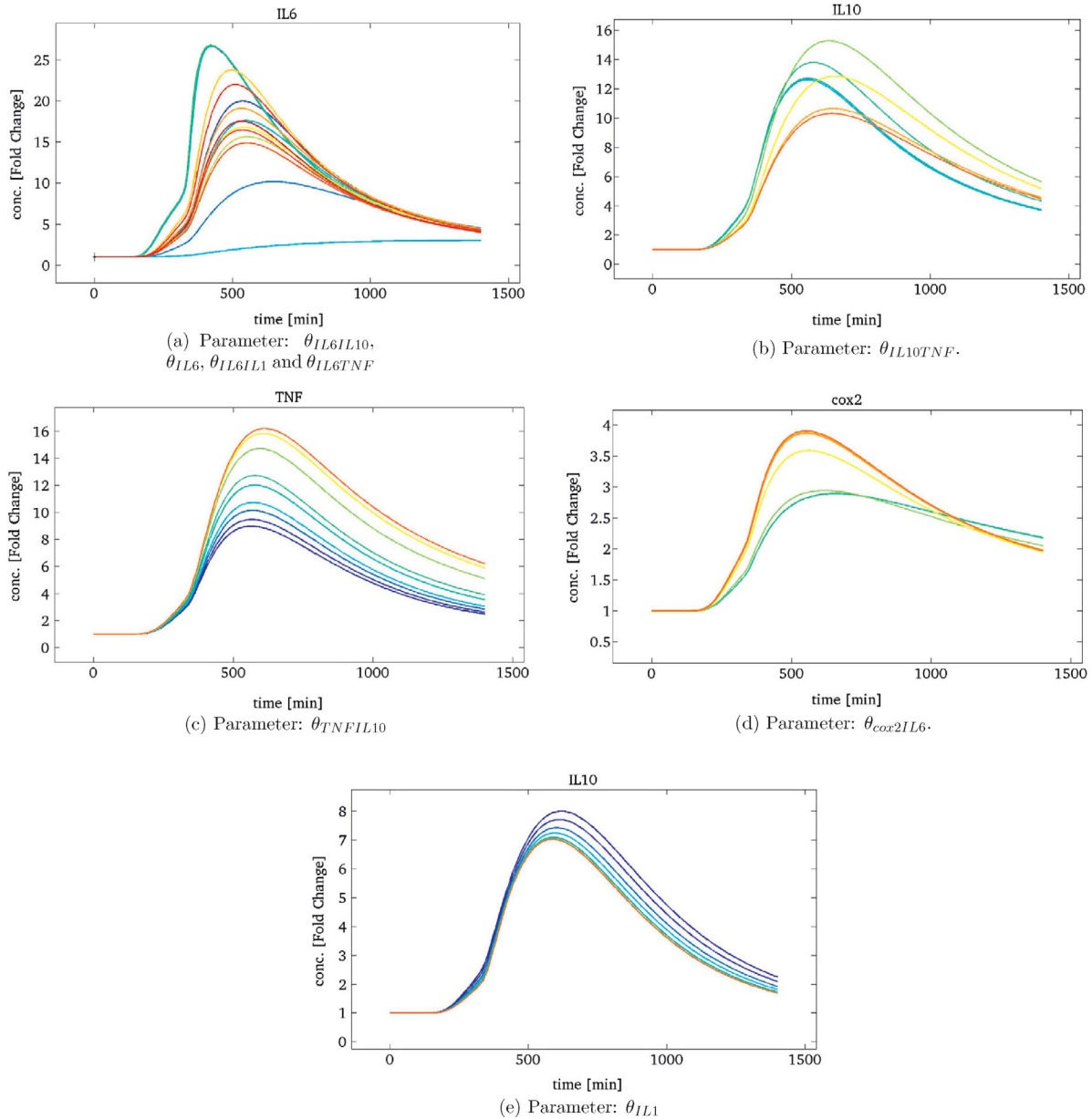


**Fig. 9.** Model predictions for IL-6 (a), IL-10 (b and e), TNF (c) and cox2 (d) gene expression data in IL10R KO (a and b), IL1R KO (c), IL6R KO (d) and IL1 KO (e) mice. Parameter vectors were chosen along the profile likelihoods of the to be identified parameters (see subcaption).

Therefore it would be most informative to modify the heat stress protocol such that mice are sacrificed at times after HD, for future experiments. Since mice have an individual heating and cooling rate, no specific time point can be suggested. Therefore we suggest to sacrifice the mice at the first time point  $T_c > 34$  °C after HD in prospective experiments.

## 5. Including TNFR KO data

### 5.1. Experimental data

Following the suggestions of the empirical Bayesian OED method and the trajectory OED method, we measured IL-10, IL-1 and TNF gene expression in TNFR KO mice. Tissue samples were extracted at  $T_{c,max}$ , RTB and HD. The corresponding time points were calculated from the averaged temperature profile of the TNFR KO mice to  $T_{c,max}$  ( $t = 263$  min), RTB ( $t = 290$  min) and HD

( $t = 427$  min) and the gene expression data are summarized in Table 4. Incorporating the TNFR KO data in the model calibration resulted in a still good data-to-model agreement for both the WT data, see Fig. 7a and the TNFR KO data, see Fig. 7b. Again for the WT data, the fitting lies within the confidence interval in almost every data point. Only IL-1 at HD is considerably larger than the model predictions, suggesting a possible IL-1 activation by TNF, as reported by [30], since the fitting of the TNFR KO data captures the trend of IL-1 almost perfectly. The TNF and IL-10 dynamics in the TNFR KO experiment are well enough captured. Identifiability analysis on the newly estimated parameters by calculating the profile likelihood is illustrated in Fig. 8. Five new parameters could be identified, namely  $\theta_{cox2IL10}$ ,  $\theta_{IL10}$ ,  $k\theta_{TNFM}$ ,  $\theta_{cox2}$  and  $\theta_{MTNF}$ , making a total of 8 out of 19 parameters identifiable and leaving 11 out of 19 non-identifiabilities. Especially the likelihood profiles of  $\theta_{IL6IL10}$ ,  $\theta_{IL6}$ ,  $\theta_{IL6TNF}$  and  $\theta_{cox2IL6}$  did not change incorporating the new data. This is not surprising since they are all affiliated with

IL-6 dynamics for which no new data were acquired. Additionally, including the TNFR KO data opens up possibilities to reduce the model. In general, whether a model should be reduced depends on the biological issue of the model. Here, the focus lies on explaining the cytokine interactions and explaining their dynamics in the hypothalamus. Therefore model reduction becomes feasible.

The profile likelihoods of  $\theta_{IL1IL10}$  and  $\theta_{MIL10}$  in Fig. 8 have both their minimum of the cost function at their upper bound ( $ub = 10^3$ ). Considering the structure of the inhibition of  $x_j$

$$\frac{\theta_{x_j,IL10}}{\theta_{x_j,IL10} + IL10}, \quad (34)$$

the inhibiting effect depends on the concentration of IL-10 and the inhibition constant  $\theta_{x_j,IL10}$ . The larger  $\theta_{x_j,IL10}$  the smaller the inhibiting effect for a constant concentration of IL-10. If  $\theta_{x_j,IL10} \gg IL10$  holds for all times the inhibition  $\frac{\theta_{x_j,IL10}}{\theta_{x_j,IL10} + IL10} \approx 1$  becomes negligible and can be

replaced by one in the ODE equations. Hence, the model can be reduced by  $\theta_{IL1IL10}$  and  $\theta_{MIL10}$  ignoring the inhibitory effects of IL-10 to IL-1 and the activated black box. The fitting results and the value of the objective function did not change, confirming that the reduced model is able to describe the dynamics of the system without loss of accuracy. The model reduction suggests that IL-10 inhibition of IL-1 and the activated black box are negligible compared to the other interactions during the inflammatory response in the hypothalamus. Additionally, parameter ++MIL1, whose profile likelihood was just below the threshold, now becomes identifiable exceeding the threshold at the upper bound and making a total of 9 out of 17 parameters identifiable. Since the impact of the reduced parameters is negligible, model reduction helps to resolve parameter identifiabilities that were nearly identifiable before without loss of fitting accuracy. Moreover, the reduction supported by the experimental data also improved the biological appropriateness of the model by identifying interactions that are not biologically relevant; insights that were not obvious at the initial stage of building the model.

To resolve the remaining non-identifiabilities *in silico* experiments of IL1 KO, IL1R KO, TNFR KO, IL6 KO, IL6R KO, IL10 KO and IL10R KO were conducted and analyzed with OED to find the most informative perturbation. The temperature profile of the WT mice served as input temperature and no specific time points were considered. Trajectories along profile likelihoods of non-identifiable parameters were simulated to visualize the highest variability in the *in silico* experiments. IL10R KO turned out to be the most informative experiment. It showed the highest variability in the trajectories for IL-6 to identify  $\theta_{IL6IL10}$ ,  $\theta_{IL6}$ ,  $\theta_{IL6IL1}$  and  $\theta_{IL6TNF}$  (Fig. 8 and for IL-10 to identify  $\theta_{IL10TNF}$  (Fig. 9b). Furthermore it is suggested to measure TNF in IL1R KO mice to identify  $\theta_{TNFIL10}$  (Fig. 9b) and cox-2 in IL6R KO mice to identify  $\theta_{cox2IL6}$  (Fig. 9d). Last but not least IL-10 in IL1 KO mice was proposed for  $\theta_{IL1}$ , showing the least variability compared to the other parameters and thus making it the most difficult parameter to identify (Fig. 9e). For all experiments it is suggested to measure the cytokines at the time point of the largest spread. For most cytokines this is the case at times after HD, agreeing with the suggestion to measure at e.g., the first time point  $T_c > 34^\circ\text{C}$  after HD.

## 6. Conclusion

After developing a mathematical model of the liver [4] we extended the emphasis on the thermoregulatory center in the brain, the hypothalamus. Based on previous studies we tested the hypothesis that denatured proteins are the main initiator of the network of HSP, cytokines and COX and considered effects of tissue damage, reactive oxidative species and endotoxins (LPS) negligible. HSP, TNF- $\alpha$ , IL-1, IL-6, IL-10 and cox-2 were secreted by an unspecified

black box of activated macrophages and monocytes and were considered the primary regulators of the immune response. The interactive network is supported by literature, however, relations among species and are not exactly known and need to be experimentally validated. Network interactions were modeled with ODEs consisting of mass action kinetics and Michaelis–Menten functions.

The model was calibrated to mRNA accumulation in the hypothalamus provided in [6]. No protein data were measured but one would expect mRNA to change prior to protein expression. The model could accurately describe the mRNA data, supporting the hypothesis of DP as main initiator. However, the  $T_c$  changes at 24 h could not be explained with the considered species in the model, showing all gene expression back to baseline at 24 h. The fever might be a delayed response to the highly elevated cytokines at HD but it is more likely that other potential mediators, e.g., chemokines [6] trigger the  $T_c$  changes. Chemokines have been shown to regulate fever in response to LPS, but their function in HS remains unknown and needs to be further investigated.

After parameter estimation a good fit was obtained and uncertainty and identifiability of parameters were calculated by means of profile likelihood. Identifiability analysis revealed difficulties in unique parameter estimation in form of non-identifiabilities. Only 3 out of 19 parameters were identifiable within a 95% confidence interval which suggested to start an iterative cycle of identifiability analysis, OED and new data collection. The empirical Bayesian and trajectory OED methods, which are robust to non-identifiable parameters helped to decide on measurements of IL6 and TNFR KO experiments stored in a tissue bank. Within this step we presented a new method to calculate a prior in the empirical Bayesian design, which is weighted according to the profile likelihoods. IL-10, TNF- $\alpha$  and IL-1 were found to be the most informative observables in TNFR KO mice for parameter estimation and gene expression changes were measured from hypothalamus tissue samples for the said cytokines. The model was re-calibrated using the WT and the novel TNFR KO data and five more parameters could be identified. The new data suggested that IL-10 inhibition on activated macrophages and on IL-1 is negligible and the model was reduced accordingly. Model reductions further improved the number of identifiable parameters. OED with *in silico* cytokine and cytokine receptor knock out experiments suggested to measure IL-6 and IL-10 gene expression in IL10R KO HS experiments at time points after HD, to identify five of the remaining eight parameters.

## Acknowledgments

The opinions or assertions contained herein are the private views of the authors and are not to be construed as official or as reflecting the views of the Army or the Department of Defense.

In conducting the research described in this report, the investigators adhered to the “Guide for Care and Use of Laboratory Animals” as prepared by the Committee on Care and Use of Laboratory Animals of the Institute of Laboratory Animal Resources, National Research Council.

Citations of commercial organizations and trade names in this report do not constitute an official Department of the Army endorsement or approval of the products or services of these organizations.

This work was supported in part by the Institute for Collaborative Biotechnologies through Grant W911NF-09-0001 from the U.S. Army Research Office.

## References

- [1] L.R. Leon III, C.J. Gordon, B.G. Helwig, D.M. Rufolo, M.D. Blaha, Thermoregulatory, behavioral, and metabolic responses to heatstroke in a conscious mouse model, *Am. J. Physiol.-Reg.* 1299 (1) (2010) 241–248.

- [2] M.N. Sawka, L.R. Leon, S.J. Montain, L.A. Sonnadoi, Integrated physiological mechanisms of exercise performance, adaptation, and maladaptation to heat stress, *Compr. Physiol.* 1 (2011) 1883–1928.
- [3] L.R. Leon, D.A. DuBose, C.W. Mason, Heat stress induces a biphasic thermoregulatory response in mice, *Am. J. Physiol.-Reg.* 1 288 (1) (2005) 197–204.
- [4] M. Rodriguez-Fernandez, B. Grosman, T.M. Yuraszcek, B.G. Helwig, L.R. Leon, F.J. Doyle III, Modeling the intra- and extracellular cytokine signaling pathway under heat stroke in the liver, *PLoS ONE* 8 (9) (2013) e73393.
- [5] L.R. Leon, Heat stroke and cytokines, *Prog. Brain Res.* 162 (2007) 481–524.
- [6] J.C. Biedenkapp, L.R. Leon, Increased cytokine and chemokine gene expression in the CNS of mice during heat stroke recovery, *Am. J. Physiol.-Reg.* 1 305 (2013) 978–986.
- [7] J. Boulant, Role of the preoptic-anterior hypothalamus in thermoregulation and fever, *Clin. Infect. Dis.* 31 (2000) 157–161.
- [8] H.T. Hammel, D.C. Jackson, J.A.J. Stolwijk, J.D. Hardy, S.B. Stromme, Temperature regulation by hypothalamic proportional control with an adjustable set point, *J. Appl. Physiol.* 18 (6) (1963) 1146–1154.
- [9] A. Raue, C. Kreutz, T. Maiwald, U. Klingmüller, J. Timmer, Addressing parameter identifiability by model-based experimentation, *IET Syst. Biol.* 5 (2) (2011) 120–130.
- [10] A. Raue, C. Kreutz, T. Maiwald, J. Bachmann, M. Schilling, U. Klingmüller, J. Timmer, Structural and practical identifiability analysis of partially observed dynamical models by exploiting the profile likelihood, *Bioinformatics* 25 (15) (2009) 1923–1929.
- [11] K.J. Livak, T.D. Schmittgen, Analysis of relative gene expression data using real-time quantitative PCR and the  $2^{-\Delta\Delta CT}$  method, *Methods* 25 (4) (2001) 402–408.
- [12] M. Dehbi, T. Uzzaman, E. Baturcam, A. Eldali, W. Ventura, A. Bouchama, Toll-like receptor 4 and high-mobility group box 1 are critical mediators of tissue injury and survival in a mouse model for heatstroke, *PLoS ONE* 7 (9) (2012) e44100.
- [13] Z. Szymańska, M. Zylicz, Mathematical modeling of heat shock protein synthesis in response to temperature change, *J. Theor. Biol.* 259 (3) (2009) 562–569.
- [14] A. Peper, C. Grimbergen, J. Spaan, J. Souren, R. Van Wijk, A mathematical model of the HSP70 regulation in the cell, *Int. J. Hyperther.* 14 (1998) 97–124.
- [15] A.A. Asea, *Heat Shock Proteins: Potent Mediators of Inflammation and Immunity*, vol. 1, Springer, Dordrecht, The Netherlands, 2007.
- [16] R.P.A. Wallin, A. Lundqvist, S.H. MorT, A. von Bonin, R. Kiessling, H.-G. Ljunggren, Heat-shock proteins as activators of the innate immune system, *Trends Immunol.* 23 (3) (2002) 130–135.
- [17] C.C. Chow, G. Clermont, R. Kumar, C. Lagoa, Z. Tawadrous, D. Gallo, B. Betten, J. Bartels, G. Constantine, M.P. Fink, T.R. Billiar, Y. Vodovotz, The acute inflammatory response in diverse shock states, *Shock* 24 (2005) 74–84.
- [18] F. Porcheray, S. Viaud, A.-C. Rimaniol, C. LTone, B. Samah, N. Dereuddre-Bosquet, D. Dormont, G. Gras, Macrophage activation switching: an asset for the resolution of inflammation, *Clin. Exp. Immunol.* 142 (3) (2005) 481–489.
- [19] J.B. Tatro, Endogenous antipyretics, *Clin. Infect. Dis.* 31 (2000) 190–201.
- [20] K.W. Moore, R. de Waal Malefyt, R.L. Coffman, A. O'Garra, Interleukin-10 and the interleukin-10 receptor, *Annu. Rev. Immunol.* 19 (1) (2001) 683–765.
- [21] C.A. Martin, M.E. Dorf, Differential regulation of interleukin-6, macrophage inflammatory protein-1, and JE/MCP-1 cytokine expression in macrophage cell lines, *Cell Immunol.* 135 (1) (1991) 245–258.
- [22] Y.H. Zhang, J.X. Lin, J. Vilcek, Interleukin-6 induction by tumor necrosis factor and interleukin-1 in human fibroblasts involves activation of a nuclear factor binding to a kappa b-like sequence, *Mol. Cell. Biol.* 10 (7) (1990) 3818–3823.
- [23] K. Tanabe, R. Matsushima-Nishiwaki, S. Yamaguchi, H. Iida, S. Dohi, O. Kozawa, Mechanisms of tumor necrosis factor-alpha-induced interleukin-6 synthesis in glioma cells, *J. Neuroinflam.* 7 (1) (2010) 16.
- [24] M. Roy, S. Girard, A. Larouche, H. Kadhim, G. Sebire, TNF-alpha system response in a rat model of very preterm brain injuries induced by lipopolysaccharide and/or hypoxia-ischemia, *Am. J. Obstet. Gynecol.* 201 (5) (2009) 493.e1–493.e10.
- [25] J.P. Edwards, X. Zhang, K.A. Frauwirth, D.M. Mosser, Biochemical and functional characterization of three activated macrophage populations, *J. Leukocyte Biol.* 80 (6) (2006) 1298–1307.
- [26] C. Platzer, C. Meisel, K. Vogt, M. Platzer, H.-D. Volk, Up-regulation of monocytic IL-10 by tumor necrosis factor  $\alpha$  and cAMP elevating drugs, *Int. Immunol.* 7 (4) (1995) 517–523.
- [27] C.A. Dinarello, Immunological and inflammatory functions of the interleukin-1 family, *Annu. Rev. Immunol.* 27 (1) (2009) 519–550.
- [28] M.E. Turini, R.N. DuBois, Cyclooxygenase-2: a therapeutic target, *Ann. Rev. Med.* 53 (1) (2002) 35–57.
- [29] L.R. Leon, Invited review: cytokine regulation of fever: studies using gene knock-out mice, *J. Appl. Physiol.* 92 (6) (2002) 2648–2655.
- [30] B. Conti, I. Tabarean, C. Andrei, T. Bartfai, Cytokines and fever, *Front. Biosci.* 9 (2004) 1433–1449.
- [31] C. Nilsberth, N. Hamzic, M. Norell, A. Blomqvist, Peripheral lipopolysaccharide administration induces cytokine mRNA expression in the viscera and brain of fever-refractory mice lacking microsomal prostaglandin E synthase-1, *J. Neuroendocrinol.* 21 (8) (2009) 715–721.
- [32] A.C. Hindmarsh, P.N. Brown, K.E. Grant, S.L. Lee, R. Serban, D.E. Shumaker, C.S. Woodward, SUNDIALS: Suite of nonlinear and differential/algebraic equation solvers, *ACM Trans. Math. Software* 31 (3) (2005) 363–396.
- [33] A. Raue, M. Schilling, J. Bachmann, A. Matteson, M. Schelker, D. Kaschek, S. Hug, C. Kreutz, B.D. Harms, F.J. Theis, U. Klingmüller, J. Timmer, Lessons learned from quantitative dynamical modeling in systems biology, *PLoS ONE* 8 (9) (2013) e74335.
- [34] A. Raue, V. Becker, U. Klingmüller, J. Timmer, Identifiability and observability analysis for experimental design in nonlinear dynamical models, *Chaos* 20 (4) (2010) 045105.
- [35] C. Kreutz, J. Timmer, Systems biology: experimental design, *FEBS J.* 276 (4) (2009) 923–942.
- [36] F. He, M. Brown, H. Yue, Maximin and Bayesian robust experimental design for measurement set selection in modelling biochemical regulatory systems, *Int. J. Robust Nonlinear* 20 (9) (2010) 1059–1078.
- [37] K. Chaloner, I. Verdinelli, Bayesian experimental design: a review, *Stat. Sci.* 10 (1995) 273–304.
- [38] M. Rodriguez-Fernandez, J.R. Banga, F.J. Doyle III, Novel global sensitivity analysis methodology accounting for the crucial role of the distribution of input parameters: application to systems biology models, *Int. J. Robust Nonlinear* 22 (10) (2012) 1082–1102.
- [39] B. Steiert, A. Raue, J. Timmer, C. Kreutz, Experimental design for parameter estimation of gene regulatory networks, *PLoS ONE* 7 (7) (2012) e40052.